

# FastVID: Dynamic Density Pruning for Fast Video Large Language Models

Leqi Shen<sup>1,2\*</sup> Guoqiang Gong<sup>3†</sup> Tao He<sup>4,5</sup> Yifeng Zhang<sup>3</sup> Pengzhang Liu<sup>3</sup>  
 Sicheng Zhao<sup>2‡</sup> Guiguang Ding<sup>1,2‡</sup>

<sup>1</sup> School of Software, Tsinghua University <sup>2</sup> BNRist, Tsinghua University

<sup>3</sup> JD.com <sup>4</sup> GRG Banking Equipment Co., Ltd. <sup>5</sup> South China University of Technology

## Abstract

Video Large Language Models have demonstrated strong video understanding capabilities, yet their practical deployment is hindered by substantial inference costs caused by redundant video tokens. Existing pruning techniques fail to fully exploit the spatiotemporal redundancy inherent in video data. To bridge this gap, we perform a systematic analysis of video redundancy from two perspectives: temporal context and visual context. Leveraging these insights, we propose Dynamic Density Pruning for Fast Video LLMs termed FastVID. Specifically, FastVID dynamically partitions videos into temporally ordered segments to preserve temporal structure and applies a density-based token pruning strategy to maintain essential visual information. Our method significantly reduces computational overhead while maintaining temporal and visual integrity. Extensive evaluations show that FastVID achieves state-of-the-art performance across various short- and long-video benchmarks on leading Video LLMs, including LLaVA-OneVision and LLaVA-Video. Notably, on LLaVA-OneVision-7B, FastVID effectively prunes **90.3%** of video tokens, reduces FLOPs to **8.3%**, and accelerates the prefilling stage by **7.1×**, while maintaining **98.0%** of the original accuracy. The code is available at <https://github.com/LunarShen/FastVID>.

## 1 Introduction

Video Large Language Models (Video LLMs) [6, 19, 16, 47, 37] have shown strong performance in video understanding but incur substantial inference costs. While several methods [31, 24, 40, 15, 30, 49] explore training-time compression to mitigate this issue, they often require expensive retraining. In this work, we focus on an inference-time acceleration strategy that enhances efficiency without requiring additional training.

This computational burden is primarily caused by the high volume of video tokens, making effective token compression essential. While prior image compression methods [5, 28, 46, 42, 4] reduce redundancy within a single image, they fail to exploit temporal dependencies across frames. As a result, the nature of video redundancy remains underexplored. In this work, we systematically analyze video redundancy from two key perspectives: *temporal context* and *visual context*.

Temporal context is fundamental to video understanding, as the order and continuity of frames directly influence semantic interpretation. As depicted in Figure 1(a), disrupting frame order (shuffled) or omitting frames (incomplete) leads to incorrect comprehension, highlighting the necessity of preserving temporal structure. To achieve this, we segment the video into temporally ordered segments, grouping highly similar consecutive frames. Pruning is applied within each high-redundancy segment but not across segments, preserving the essential temporal structure for accurate video understanding.

To maintain visual context, redundant tokens within each segment must be effectively merged. A state-of-the-art method VisionZip [42] applies uniform token sampling followed by merging redundant

\*Work done during an internship at JD.com. †Project lead. ‡ Corresponding authors.

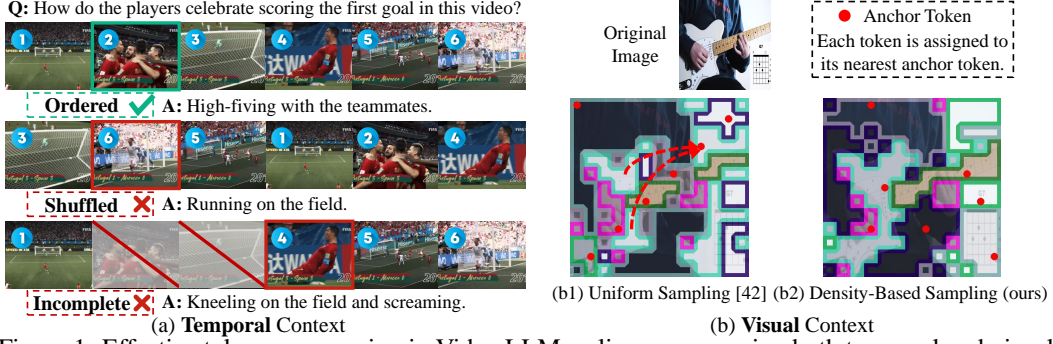


Figure 1: Effective token compression in Video LLMs relies on preserving both temporal and visual context. (a) shows the impact of temporal disruptions, emphasizing the importance of temporal structure preservation. (b) show the effects of different token selection strategies for visual merging, where patches that share the same inner and border color are merged. Density-based Sampling retains both distinctive and representative context while effectively reducing redundancy.

tokens [4] as shown in Figure 1(b1). However, its token selection strategy is content-agnostic, potentially leading to the loss of important details, such as the guitar body being incorrectly merged with the background. To address this, we propose a density-based token sampling in Figure 1(b2). Specifically, high-density tokens, surrounded by numerous similar tokens, serve as candidates for selection. We select density peak tokens as anchors, which have a higher density than their neighbors and by a relatively large distance from tokens with higher densities [26]. This strategy ensures that the selected tokens are both representative and distinctive, effectively preserving segment visual context while reducing redundancy.

Building upon these insights, we propose Dynamic Density Pruning for **Fast VIDeo** LLMs, minimizing spatiotemporal redundancy while preserving essential semantics. We begin with Dynamic Temporal Segmentation, which adaptively partitions videos into segments. Within each segment, we introduce Density Spatiotemporal Pruning to retain both global visual context and salient details. FastVID significantly accelerates inference while preserving both temporal and visual integrity.

To evaluate the generalization capability of our approach, we evaluate it on two leading Video LLMs, LLaVA-OneVision [16] and LLaVA-Video [47]. To further validate its effectiveness, we perform extensive experiments on MVBench [18], LongVideoBench [38], MLVU [48], and VideoMME [11]. These benchmarks cover a wide range of video complexities and durations, ensuring a comprehensive evaluation. Notably, on LLaVA-OneVision-7B, FastVID effectively prunes **90.3%** of video tokens, reduces FLOPs to **8.3%**, and accelerates the prefilling stage by **7.1 $\times$** , while maintaining **98.0%** of the original accuracy across all benchmarks.

The main contributions are summarized as follows: (1) We analyze Video LLM compression from both temporal and visual context perspectives, emphasizing the importance of maintaining temporal and visual integrity. (2) We propose FastVID, a novel pruning framework that employs Dynamic Temporal Segmentation to partition videos into temporally ordered segments and Density Spatiotemporal Pruning to retain global segment information and key details. (3) Our FastVID achieves state-of-the-art performance across diverse video benchmarks and maintains robust accuracy even under extreme compression.

## 2 Related Work

**Video LLMs.** With the rapid advancement of LMMs [1, 7, 34] and MLLMs [35, 21, 22, 17, 3, 23], there has been growing interest in Video LLMs. These models can be categorized based on how they process video tokens: general Video LLMs and Video LLMs with training-time compression.

General Video LLMs [20, 6, 19, 16, 47, 37] directly process raw video tokens or apply pooling. Video-LLaVA [19] leverages shared projection layers to obtain unified visual representations. LLaVA-OneVision [16] demonstrates strong video understanding through task transfer from images. LLaVA-Video [47] creates a high-quality synthetic dataset for video instruction-following. To better capture the spatiotemporal structure of video, some models [47, 37] introduce additional designs for video

positional information. LLaVA-Video<sup>1</sup> introduces newline tokens to distinguish spatial and temporal positions effectively.

Video LLMs with training-time compression [31, 24, 40, 15, 30, 49] aim to significantly reduce the number of video tokens, enabling longer video sequences. PLLaVA [40] introduces an adaptive average structure pooling to extend image LLMs. Video-ChatGPT [24] extracts both spatial and temporal features through temporal and spatial pooling respectively. Chat-UniVi [15] progressively clusters visual tokens and provides multi-scale features. LongVU [30] employs cross-modal query and inter-frame dependencies to adaptively reduce video redundancy. Apollo [49] explores scaling consistency and uses the Perceiver Resampler [14].

However, general Video LLMs remain the dominant paradigm, with LLaVA-OneVision being widely adopted due to its adaptability and superior performance. Therefore, we focus on inference-time acceleration for general Video LLMs. To evaluate our method, we select LLaVA-OneVision and LLaVA-Video as representative models.

**Token Compression.** Token compression has emerged as an effective approach to reduce computational complexity in transformer architectures, such as ViT [9] and CLIP [25]. ToMe [4] progressively merges fixed spatial tokens, while TempMe [29] extends this concept by merging neighboring clips to minimize temporal redundancy.

Recent studies [5, 28, 46, 42, 4, 39] primarily focus on spatial token reduction to accelerate Image LLMs. FastV [5] selects text-relevant tokens at shallow layers of the LLM. LLaVA-PruMerge [28] uses attention scores from the [CLS] token to prune spatial redundancy. SparseVLM [46] proposes a token recycling strategy to aggregate and reconstruct tokens to be pruned. VisionZip [42] reduces visual redundancy in the vision encoders. However, these methods overlook the temporal relationships across frames.

Due to the high volume of video tokens in Video LLMs, recent video compression methods [12, 33, 13] have gained increasing attention. FrameFusion [12] applies both merging and pruning across successive shallow LLM layers, but repeated pruning operations adversely affect overall efficiency. DyCoke [33] merges tokens across frames and applies dynamic KV cache reduction. However, its pruning during the prefilling stage struggles to achieve substantial token reduction while maintaining accuracy. PruneVID [13] clusters video tokens and selects those most relevant to query tokens, but this dependency on clustering introduces significant latency during compression. Despite these advances, efficient and accurate pruning under large token reduction remains unsolved.

In this paper, we focus on preserving temporal and visual context for spatiotemporal token pruning at the prefilling stage. By reducing video tokens before LLM processing, our FastVID significantly enhances computational efficiency while facilitating easy deployment, including compatibility with FlashAttention [8], KV cache, and a plug-and-play design for seamless integration into existing Video LLMs. Our method achieves robust performance even under extreme compression rates, offering a practical solution for fast Video LLMs.

### 3 Methodology

#### 3.1 FastVID

Video LLMs face significant inference challenges due to the large number of frames in a video and the numerous vision tokens within each frame. Typically, the total token count often exceeds the LLM’s context length, making direct processing computationally infeasible. Although uniform frame sampling and token pooling methods are commonly employed to reduce complexity, they still leave a substantial number of redundant video tokens (*e.g.*,  $32 \times 196 = 6272$  video tokens in LLaVA-OneVision [16]).

To address these limitations, we propose FastVID, a novel method that accelerates inference by reducing redundant tokens while preserving critical temporal and visual context. First, we introduce Dynamic Temporal Segmentation (DySeg) in Section 3.2, which partitions a video into temporally ordered segments with high redundancy. Within each segment, we introduce Density Spatiotemporal Pruning (STPrune) in Section 3.3, which retains essential visual context and salient details.

---

<sup>1</sup><https://github.com/LLaVA-VL/LLaVA-NeXT>

Figure 2 presents an overview of FastVID. Given an input video,  $F$  frames are uniformly sampled (e.g., 32 in LLaVA-OneVision, 64 in LLaVA-Video). Each frame is individually processed by the vision encoder. The extracted tokens are projected and pooled into a video token sequence. With FastVID, we effectively eliminate redundant tokens while preserving critical information. Specifically, DySeg dynamically partitions video tokens into temporally ordered, high-redundancy segments, while STPrune performs density-based pruning within each segment, enhancing efficiency without loss of key information. The final retained video tokens, combined with query tokens, is then fed into the LLM to generate the response.

### 3.2 Dynamic Temporal Segmentation

As shown in Figure 3(b) and 3(c), there are two common static segmentation methods for sampled frame sequences. In Figure 3(b), Fixed-interval Segmentation partitions the sequence into segments of a fixed length, preserving temporal order but potentially grouping visually dissimilar frames. Figure 3(c) shows Cluster-based Segmentation, where frames are grouped into three clusters based on frame similarity. However, it suffers from a predefined cluster number, leading to ineffective segmentation when video complexity varies. As a result, the first segment contains similar objects but different scenes. Furthermore, clustering may disrupt the temporal order by ignoring critical temporal information, such as omitting key frames (e.g., the 9th frame) and incorrectly grouping frames from different time periods into the first segment.

To address the limitations of static methods, we propose Dynamic Temporal Segmentation, a simple yet effective method that adaptively refines segment boundaries according to video complexity. DySeg achieves both temporal structure and high intra-segment similarity, generating fewer partitions for simple scenes and finer ones for more complex scenes.

To enable effective pruning, DySeg promotes high spatiotemporal redundancy within each segment by minimizing similarity between adjacent segments. Thus, we segment the video based on transition similarity between adjacent frames. Specifically, we utilize global frame features  $\mathbf{f}$  to compute the cosine similarity:

$$t_i = \cos(\mathbf{f}_i, \mathbf{f}_{i+1}), \quad i = 1, \dots, F-1, \\ \mathbf{T} = \{t_1, t_2, \dots, t_{F-1}\}, \quad (1)$$

where  $t_i$  denotes the transition similarity between the  $i$ -th and  $(i+1)$ -th frame.  $\mathbf{T}$  denotes the  $F-1$  transition similarities for  $F$  sampled frames. To achieve fine-grained segmentation, we select transitions that satisfy the following conditions:

$$\mathbf{S}_1 = \arg \min_{c-1} \mathbf{T}, \quad \mathbf{S}_2 = \{i \mid t_i < \tau, t_i \in \mathbf{T}\}, \\ \mathbf{S} = \mathbf{S}_1 \cup \mathbf{S}_2, \quad (2)$$

where  $c$  denotes the minimum number of segments and  $\tau$  denotes the threshold for transition similarity.  $\mathbf{S}_1$  denotes the  $c-1$  least similar frame transitions, while  $\mathbf{S}_2$  denotes transitions where similarity falls below a fixed threshold  $\tau$ . Each transition in the union  $\mathbf{S}$  marks a boundary between segments. In simple videos with minimal shot transitions,  $\mathbf{S}_2$  is often empty. In such cases,  $\mathbf{S}_1$  enables finer segmentation by distinguishing subtle temporal changes. For complex videos,  $\mathbf{S}_1$  is typically a subset of  $\mathbf{S}_2$ , where  $\mathbf{S}_2$  ensures that adjacent frames with similarity below  $\tau$  are assigned to different segments. In Figure 3(d), our DySeg effectively segments videos by dynamically adjusting granularity in a simple yet effective manner, outperforming Fixed-interval and Clustering-based methods.

### 3.3 Density Spatiotemporal Pruning

After obtaining segments with highly similar frames, we introduce STPrune to reduce redundant tokens. It consists of two key modules: Density-based Token Merging (DTM) for segment visual context and Attention-based Token Selection (ATS) for salient details. For a segment of  $P$  frames, we

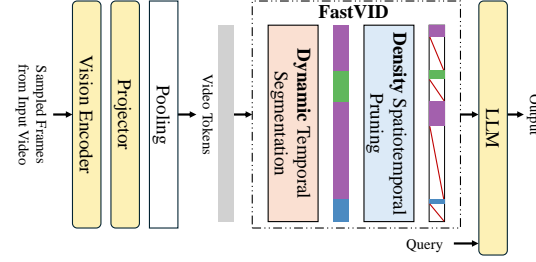


Figure 2: The overview of our FastVID.

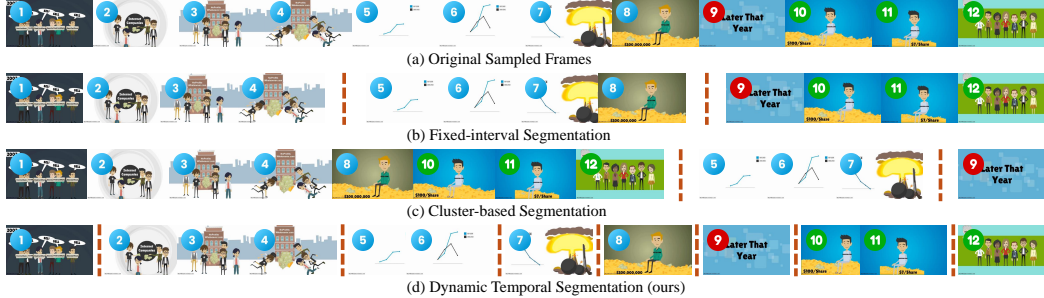


Figure 3: Visualization of different segmentation methods on 12 sampled frames from a video example. (b) Fixed-interval Segmentation struggles to maintain high intra-segment similarity, leading to visually diverse frames within the same segment. (c) Cluster-based Segmentation disrupts temporal order, grouping frames from different time periods to the same segment. (d) Our DySeg adaptively partitions the video, preserving both temporal structure and high intra-segment similarity. Please refer to Table 6 for a detailed quantitative comparison.

retain  $rPN$  tokens in total, where  $N$  is the number of tokens per frame, and  $r$  denotes the retention ratio. These tokens are generated by DTM and ATS. Specifically,  $drFN$  tokens are generated by DTM and  $(1 - d)rFN$  tokens are generated by ATS, where  $d$  controls the token allocation between the two modules.

**Density-based Token Merging.** For segment visual context, we first identify anchor tokens and to-be-merged tokens. Selecting anchor tokens from the entire segment would disrupt their spatial relationships, as anchor tokens corresponding to different components of the same object might be distributed across multiple frames. To mitigate this, we restrict anchor token selection to specific frames. Specifically, we sample anchor frames at a fixed interval  $p$  and select anchor tokens from these frames. The remaining tokens in the segment are treated as to-be-merged tokens. Specifically, the number of anchor frames is  $\lceil P/p \rceil$ . From each anchor frame,  $drPN/\lceil P/p \rceil$  tokens are selected as anchor tokens. Please see Figure 5 for a visualization of DTM applied to video segments.

To further clarify DTM, Figure 4(b) illustrates DTM when the segment length is 1 and shows that it consists of three key steps. First, we follow density peaks clustering algorithms [26, 10] to compute the density score. For each token in the anchor frame  $[v_1, v_2, \dots, v_N]$ , we calculate its local density  $\rho_i$  and its distance to the closest higher-density token  $\delta_i$ , obtaining the final density score  $\rho_i \times \delta_i$ :

$$\rho_i = \exp\left(-\frac{1}{k} \sum_{v_j \in \text{kNN}(v_i)} d(v_i, v_j)^2\right), \quad (3)$$

$$\delta_i = \begin{cases} \min_{j: \rho_j > \rho_i} d(v_i, v_j), & \text{if } \exists j \text{ s.t. } \rho_j > \rho_i \\ \max_j d(v_i, v_j), & \text{otherwise} \end{cases} \quad (4)$$

where  $d(v_i, v_j)$  denotes the Euclidean distance. Density peak tokens with high  $\rho_i \times \delta_i$  serve as anchor tokens, indicating that they are surrounded by neighbors with lower local density while remaining relatively distant from other high-density tokens. This selection ensures that anchor tokens are both representative and distinctive. Next, for each anchor frame, Similarity-based Assignment assigns each token in the segment to the nearest anchor token using cosine similarity. Finally, we apply Anchor-centric Aggregation to merge the assigned tokens into their respective anchors, preserving key visual structures through representative tokens. For an anchor  $a$  and its associated tokens  $[b_1, \dots, b_n]$ , the updated  $a^*$  is computed as:

$$a^* = \alpha a + \frac{1 - \alpha}{n} \sum_{i=1}^n b_i, \quad (5)$$

where  $\alpha$  controls the balance between the anchor token and its associated tokens. In Figure 4, we compare our DTM with Cluster-based Token Merging. In LLMs, RoPE [32] encodes relative positional relationships between tokens, making positional information essential for maintaining the spatiotemporal structure of video tokens. While prior methods [13] rely on Cluster-based Token

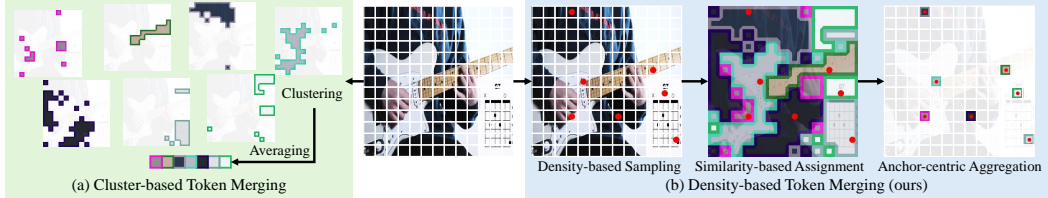


Figure 4: Comparison of DTM and Cluster-based Token Merging. (a) Cluster-based methods aggregate tokens within each cluster and concatenate them, leading to a loss of positional information and disruption of the spatiotemporal structure in video data. (b) Our DTM updates anchor tokens while preserving their original positional information, maintaining structural coherence. Please refer to Table 5 for a detailed quantitative comparison.

Merging, they discard positional information, causing RoPE to struggle with encoding spatiotemporal structure. In contrast, our DTM maintains the positional information of merged tokens, enhancing visual context understanding.

Overall, our DTM offers three key advantages: (1) Density-based Sampling selects density peak tokens as anchors, ensuring representative visual context. (2) We maintain the original positional information of updated anchor tokens, preserving spatiotemporal structure. (3) Anchor-centric Aggregation emphasizes representative tokens, enhancing feature representation.

**Attention-based Token Selection.** In addition to segment visual context obtained through DTM, we introduce ATS to capture salient visual details.

Motivated by previous studies [28, 42, 36, 45], we utilize [CLS] attention scores to identify salient visual information. However, in Video LLMs, which commonly use SigLIP [43] as their vision encoder, [CLS] attention scores cannot be obtained. This is because Video LLMs utilize the penultimate layer of SigLIP, omitting the SigLIP head where the [CLS] token is generated. To overcome this, we reintegrate a pretrained SigLIP head into the vision encoder, allowing the model to compute [CLS] attention scores. Since the SigLIP head is lightweight (15.2M parameters), this modification incurs minimal computational overhead compared to the full Video LLM.

Specifically, we extract the [CLS] attention score from the pretrained SigLIP head,  $\mathbf{A} \in \mathbb{R}^{H \times W}$ , where  $H$  and  $W$  are the spatial dimensions of frame tokens. Since Video LLMs incorporate pooling (see Figure 2), we apply the same operation to  $\mathbf{A}$ , resulting in  $\bar{\mathbf{A}} \in \mathbb{R}^{\bar{H} \times \bar{W}}$ , where  $\bar{H}$  and  $\bar{W}$  are the pooled spatial dimensions. Finally, for each frame, we select the top  $(1 - d)rN$  tokens with the highest attention scores to preserve critical visual details.

## 4 Experiments

### 4.1 Experimental Settings

**Benchmarks.** We evaluate our method on several widely used video understanding benchmarks: MVBench [18, 27], LongVideoBench [38], MLVU [48], and VideoMME (wo sub.) [11]. Specifically, VideoMME is officially divided into short, medium, and long subsets. These benchmarks contain videos of varying durations and complex scenarios, providing a comprehensive evaluation of our method’s effectiveness and generalization.

**Implementation Details.** We apply our method to two representative Video LLMs: LLaVA-OneVision-7B [16] is a general Video LLM, while LLaVA-Video-7B [47] employs newline tokens based on positional information of video tokens. These models encompass different architectural characteristics, ensuring a robust evaluation of our approach. Unless otherwise specified, we adopt the hyperparameter setting  $c = 8, \tau = 0.9, d = 0.4, p = 4, \alpha = 0.6$  for all experiments. For LLaVA-OneVision, 32 sampled frames generate a  $32 \times 196$  token input to the LLM. We test with  $r \in \{25\%, 20\%, 15\%, 10\%\}$ . For LLaVA-Video, 64 sampled frames generate a  $64 \times 169$  token input. We test with  $r \in \{25\%, 10\%\}$ . We conduct all evaluations using LMMs-Eval [44] on A100 GPUs.

**Compared Baselines.** (1) For image compression, we adopt both the widely used classic method FastV [5] and the current state-of-the-art approach VisionZip [42]. VisionZip prunes tokens in the

Table 1: Comparison of state-of-the-art methods on LLaVA-OneVision [16]. The A%/B% retention ratio indicates that A% of the LLM input tokens are retained, and subsequently compressed to B% during the LLM forward pass. The best performance among those with similar retention ratios  $R$  is highlighted in bold. TFLOPs related to video tokens are reported (see the appendix for details).

Method	Retention Ratio $R$	TFLOPs	MV Bench	Long Video Bench		MLVU	VideoMME			Avg. Acc. Score	%
				16s	1~60min		Overall	Short	Medium	Long	
Vanilla	100%	48.82	56.9	56.4	65.2	58.6	70.3	56.6	48.8	59.3	100
DyCoke [33]CVPR'25	32.5%	14.13	56.3	56.6	62.1	57.1	68.1	56.7	46.7	58.0	97.8
FastV [5]ECCV'24	100%/25%	13.45	54.7	55.5	61.5	56.2	68.0	54.6	46.0	57.0	96.1
VisionZip [42]CVPR'25	25%	10.73	53.7	51.2	58.5	54.1	61.6	53.4	47.2	54.4	91.7
VisionZip* [42]CVPR'25	25%	10.73	<b>56.6</b>	55.7	<b>64.8</b>	<b>58.0</b>	68.6	<b>57.7</b>	<b>47.7</b>	<b>58.8</b>	<b>99.1</b>
DyCoke [33]CVPR'25	25%	10.73	49.5	48.1	55.8	51.0	61.1	48.6	43.2	51.1	86.2
<b>FastVID</b>	25%	10.73	56.5	<b>56.3</b>	64.1	<b>58.0</b>	<b>69.9</b>	56.6	<b>47.7</b>	58.7	99.0
FastV [5]ECCV'24	100%/20%	11.38	54.1	56.6	61.2	56.2	66.8	54.6	47.2	57.0	96.1
VisionZip [42]CVPR'25	19.9%	8.46	53.0	50.0	57.1	53.0	60.8	51.0	47.1	53.3	90.0
VisionZip* [42]CVPR'25	19.9%	8.46	55.8	55.4	<b>64.2</b>	<b>58.0</b>	68.6	<b>57.0</b>	<b>48.3</b>	58.4	98.5
<b>FastVID</b>	19.9%	8.46	<b>56.3</b>	<b>57.1</b>	63.9	57.9	<b>69.3</b>	56.7	47.7	<b>58.8</b>	<b>99.1</b>
FastV [5]ECCV'24	100%/15%	9.35	53.2	54.9	59.8	54.7	65.1	53.4	45.7	55.7	93.9
VisionZip [42]CVPR'25	14.8%	6.23	50.3	46.9	54.4	49.5	55.8	49.3	43.3	50.3	84.8
VisionZip* [42]CVPR'25	14.8%	6.23	54.3	53.9	63.1	55.5	63.0	54.4	<b>49.1</b>	56.7	95.6
<b>FastVID</b>	14.8%	6.23	<b>56.0</b>	<b>56.2</b>	<b>63.2</b>	<b>57.7</b>	<b>69.3</b>	<b>56.2</b>	47.4	<b>58.3</b>	<b>98.3</b>
FastV [5]ECCV'24	100%/10%	7.36	51.7	52.1	57.7	52.4	60.9	51.4	45.0	53.5	90.2
VisionZip [42]CVPR'25	9.7%	4.04	44.4	43.5	51.5	46.0	50.4	45.8	41.8	46.4	78.3
VisionZip* [42]CVPR'25	9.7%	4.04	51.7	48.3	59.7	52.8	59.4	52.0	46.9	53.1	89.6
PruneVID* [13]ACL'25	10.1%	4.23	54.2	53.8	62.3	55.9	66.4	52.9	48.3	56.6	95.4
<b>FastVID</b>	9.7%	4.04	<b>55.9</b>	<b>56.3</b>	<b>62.7</b>	<b>57.3</b>	<b>67.4</b>	<b>56.0</b>	<b>48.6</b>	<b>58.1</b>	<b>98.0</b>
PruneVID [13]ACL'25	10.1%/3.9%	2.58	54.1	51.8	<b>62.3</b>	55.5	<b>67.1</b>	51.8	47.7	55.9	94.3
<b>FastVID+FastV [5]</b>	9.7%/3.6%	2.47	<b>55.0</b>	<b>53.6</b>	61.9	<b>56.3</b>	66.1	<b>54.8</b>	<b>48.1</b>	<b>56.7</b>	<b>95.6</b>

Table 2: Comparison of state-of-the-art methods on LLaVA-Video [47]. TFLOPs\* calculations include both video and newline tokens.

Method	Retention Ratio $R$	# Newline Tokens $M$	TFLOPs*	MV Bench	Long Video Bench		MLVU	VideoMME			Avg. Acc. Score	%
					Overall	Short		Overall	Short	Long		
Vanilla	100%	832	103.2	60.4	59.6	70.3	64.1	76.9	53.4	63.6	100	
DyCoke [33]CVPR'25	32.1%	256	27.1	59.3	57.9	65.7	61.6	74.6	51.1	61.1	96.1	
FastV [5]ECCV'24	100%/25%	832/568.7	29.2	58.0	<b>58.3</b>	63.9	61.0	71.3	51.0	60.3	94.8	
VisionZip [42]CVPR'25	24.9%	64	19.5	56.4	54.1	62.1	58.6	66.3	51.2	57.8	90.9	
VisionZip* [42]CVPR'25	24.9%	64	19.5	58.3	<b>58.3</b>	66.6	61.9	73.3	52.2	61.5	96.7	
DyCoke [33]CVPR'25	25%	208	20.7	50.8	53.0	56.9	56.1	65.8	48.9	54.2	85.2	
<b>FastVID*</b>	24.9%	64	19.5	59.3	<b>58.3</b>	67.7	62.6	<b>74.9</b>	52.0	62.0	97.5	
<b>FastVID</b>	24.9%	715.5	24.5	<b>59.9</b>	57.4	<b>68.6</b>	<b>63.6</b>	<b>74.9</b>	<b>53.7</b>	<b>62.4</b>	<b>98.1</b>	
FastV [5]ECCV'24	100%/10%	832/311.8	16.2	55.8	55.4	58.9	57.9	67.6	48.6	57.0	89.6	
VisionZip [42]CVPR'25	9.5%	64	7.3	46.3	46.6	52.2	49.5	54.2	44.3	48.7	76.6	
VisionZip* [42]CVPR'25	9.5%	64	7.3	56.6	53.6	61.7	58.7	67.6	50.1	57.7	90.7	
<b>FastVID*</b>	9.5%	64	7.3	58.3	56.2	63.9	59.6	70.9	50.7	59.5	93.6	
<b>FastVID</b>	9.5%	508.2	10.5	<b>58.5</b>	<b>56.5</b>	<b>64.9</b>	<b>60.7</b>	<b>71.7</b>	<b>51.2</b>	<b>60.2</b>	<b>94.7</b>	

last layer of the vision encoder, conflicting with pooling in Video LLMs and degrading performance. To address this, we implement VisionZip\*, which applies pruning after pooling. (2) For video compression, we compare two recent methods, DyCoke [33] and PruneVID [13]. Our FastVID focuses on pruning during the prefilling stage. To ensure fairness, we reimplement these baselines without pruning in the decoding stage. PruneVID applies two-stage pruning on both input tokens and the LLM's 10th layer. PruneVID\* refers to the variant that prunes only input tokens. More implementation details of these baselines are provided in the appendix.

## 4.2 Comparisons with State-of-the-Art Methods

For a comprehensive evaluation, we compare our FastVID with state-of-the-art methods on benchmarks with diverse video durations. In DyCoke, video frames are evenly divided into 4-frame segments, retaining all tokens from the first frame while pruning the rest. Consequently, its lowest retention ratio  $R$  is 25%. For other baselines, we conduct comparisons across different  $R$  values.

**Results on LLaVA-OneVision.** In Table 1, we evaluate our FastVID against other methods on LLaVA-OneVision. While FastV and VisionZip perform well at  $R = 25\%$ , but their performance declines sharply as  $R$  decreases. This indicates the limitations of spatial compression alone, which struggles to preserve essential temporal information under extreme pruning. Notably, even after pruning **90.3%** of the tokens, our FastVID preserves **98.0%** of the vanilla model's performance. To compare with PruneVID, we additionally apply FastV at the 10th layer of the LLM. FastVID+FastV achieves **95.6%** of the original accuracy at **2.47 (5.1%)** TFLOPs.

Table 3: Efficiency Comparison on LLaVA-OneVision [16]. The prefilling time, defined as the latency to the first generated token, is measured on VideoMME using an A100 GPU.

Method	# Token	TFLOPs	Prefilling Time (ms)			Avg. Acc.	
			Segmentation	Compression	LLM Forward		
Vanilla	6272 (100%)	48.82 (100%)	—	—	476.3	476.3 (1.0 $\times$ )	59.3 (100%)
PruneVID* [13]	635.6 (10.1%)	4.23 (8.7%)	5.2	32.0	64.3	101.5 (4.7 $\times$ )	56.6 (95.4%)
FastVID	<b>608 (9.7%)</b>	<b>4.04 (8.3%)</b>	<b>0.5</b>	<b>5.6</b>	<b>61.1</b>	<b>67.2 (7.1<math>\times</math>)</b>	<b>58.1 (98.0%)</b>

Table 4: Ablation Study on  $d$  in STPrune. STPrune consists of DTM and ATS. A fraction  $d$  of the retained tokens is from DTM, while the remaining  $1 - d$  is from ATS.

$d$ in STPrune	MVBench	LongVideo- Bench	MLVU	VideoMME	Avg. Acc.
0.0/ATS	55.3	55.3	62.4	55.0	96.2
0.2	55.0	53.6	62.1	56.1	95.7
0.4	55.9	<b>56.3</b>	<b>62.7</b>	<b>57.3</b>	<b>98.0</b>
0.6	55.6	54.5	62.0	56.2	96.3
0.8	<b>56.0</b>	54.9	62.6	55.6	96.7
1.0/DTM	54.1	50.1	61.5	55.9	93.5

Table 5: Ablation study on different token merging strategies. Figure 1(b1) presents Uniform. Figure 4(a) presents Cluster-based.

Token Merging	MVBench	LongVideo- Bench	MLVU	VideoMME	Avg. Acc.	LLaVA-OneVision
						LLaVA-Video
Uniform	55.0	54.7	62.0	56.4	96.2	
Cluster-based	55.6	55.2	62.4	<b>57.3</b>	97.2	
Our DTM	<b>55.9</b>	<b>56.3</b>	<b>62.7</b>	<b>57.3</b>	<b>98.0</b>	
						LLaVA-Video
Uniform	55.4	54.6	62.9	59.8	91.5	
Cluster-based	55.3	55.1	62.9	60.1	91.8	
Our DTM	<b>58.5</b>	<b>56.5</b>	<b>64.9</b>	<b>60.7</b>	<b>94.7</b>	

**Results on LLaVA-Video.** LLaVA-Video adopts a unique design by inserting newline tokens after each height-wise position in every frame, producing  $64 \times 13 \times (13 + 1)$  tokens. In Table 2, for all methods, when the positional information of retained tokens is preserved, we also retain the associated newline tokens. For a fair comparison with VisionZip, we evaluate FastVID\*, where only one newline token is retained per frame. Notably, our FastVID consistently outperforms all baselines across various retention ratios.

**Efficiency Comparison.** Table 3 compares the efficiency of our method against the state-of-the-art video compression method PruneVID. Latency and accuracy are evaluated while maintaining similar model complexity. PruneVID relies heavily on time-consuming clustering algorithms during both video segmentation and compression. In contrast, FastVID leverages transition similarity to achieve efficient segmentation. Although density score computation (see Eq. (3-4)) is time-consuming, we restrict this step to anchor frames and parallelize its execution, thereby accelerating the compression process. As a result, FastVID achieves a **7.1 $\times$**  speedup while preserving **98.0%** accuracy.

### 4.3 Ablation Study

By default, we conduct ablation studies on LLaVA-OneVision at  $r = 10\%$ . Further hyperparameter analysis is provided in the appendix.

**Ablation study on DySeg.** To compare different video segmentation methods, we present qualitative and quantitative results in Figure 3 and Table 6, respectively. In Table 6, Fixed-interval Segmentation with an interval of 4 generates  $32/4 = 8$  segments, while Cluster-based Segmentation generates 8 clusters, ensuring consistency with the minimal segment number  $c$  in our DySeg. Fixed-interval preserves temporal order between segments, whereas Cluster-based maintains intra-segment similarity. The results show that Fixed-interval outperforms Cluster-based by 1.4%, highlighting the importance of temporal structure preservation in Video LLM pruning. Additionally, high intra-segment similarity is also essential for effective pruning. Our proposed DySeg successfully integrates both advantages while enabling dynamic pruning, achieving a superior average performance of **98.0%**.

**Ablation study on STPrune.** STPrune is proposed to prune tokens within each segment and consists of two key components: DTM and ATS. DTM employs density-based sampling to merge redundant tokens, preserving segment visual context. ATS leverages [CLS] attention scores to highlight important visual details. Table 4 presents an ablation study on  $d$ , which controls the pruning distribution between DTM and ATS. The results show that ATS alone (when  $d = 0.0$ ) outperforms DTM alone (when  $d = 1.0$ ). However, the best performance is achieved at  $d = 0.4$ , demonstrating

Table 6: Ablation study on video segmentation.

Segmentation	MVBench	LongVideo- Bench	MLVU	VideoMME	Avg. Acc.
Fixed-interval	55.1	53.6	61.7	55.4	95.3
Cluster-based	53.2	53.0	61.7	54.8	93.9
Our DySeg	<b>55.9</b>	<b>56.3</b>	<b>62.7</b>	<b>57.3</b>	<b>98.0</b>

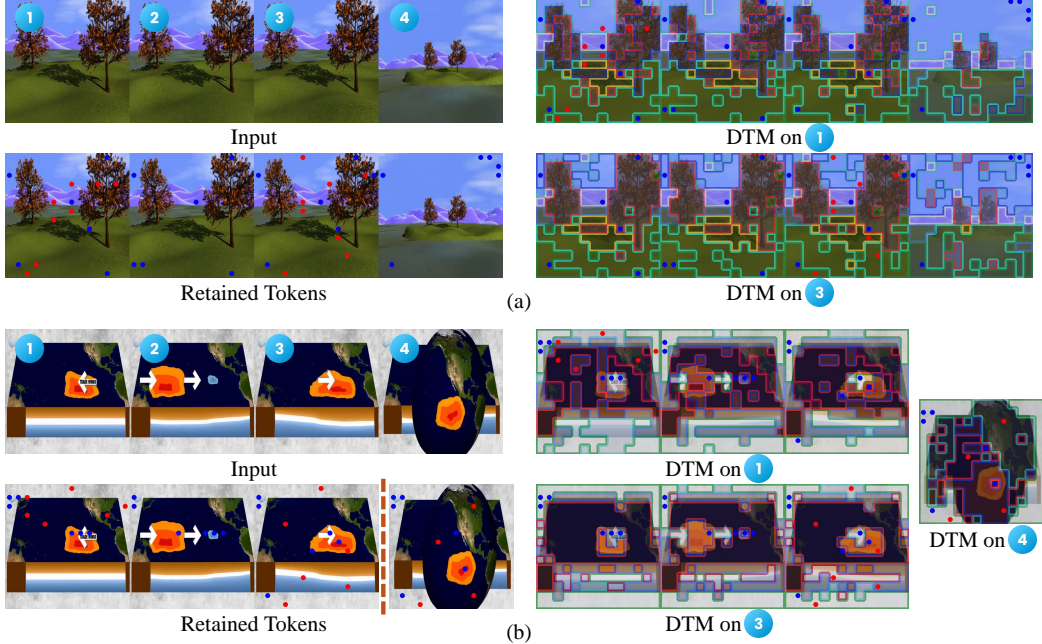


Figure 5: Visualization of FastVID with  $c = 0, \tau = 0.9, d = 0.4, p = 2$ . We retain a total of 40 tokens, including 16 tokens in DTM (highlighted in red) and 24 in ATS (highlighted in blue). In DTM, patches that share the same inner and border color are merged.

that a balanced integration of both modules is crucial for preserving essential video information. This integration boosts performance by **1.8%** and **4.5%** points over ATS and DTM alone, respectively.

**Ablation study on DTM.** In Table 5, we compare different token merging strategies for segment visual context. Uniform, used in VisionZip, selects anchor tokens in a content-agnostic manner, which limits its ability to distinguish semantically meaningful objects. Cluster-based discards essential positional information, resulting in inferior performance, particularly in LLaVA-Video. By leveraging Density-based Sampling and Anchor-centric Aggregation, our DTM achieves superior results, especially in LLaVA-Video, where DTM outperforms other methods by **2.9%**.

#### 4.4 Qualitative Results

Figure 5 visualizes the proposed DySeg and STPrune. In Figure 5(a), all frames are grouped into a single segment, with the 1st and 3rd frames selected as anchor frames, where DTM is applied. In Figure 5(b), the frames are divided into two segments, with the 1st, 3rd, and 4th frames selected as anchor frames. Blue tokens represent those selected by ATS due to high [CLS] attention. These tokens readily cluster together and do not always correspond to object regions, suggesting that while they reflect salient [CLS] information, they lack broader visual context. In contrast, DTM’s red tokens effectively aggregate visually similar content across frames, significantly reducing spatiotemporal redundancy while preserving visual context. Together, ATS and DTM offer complementary benefits for effective video compression. More qualitative results are provided in the appendix.

## 5 Conclusion

In this paper, we introduced FastVID, a novel inference-time pruning framework designed to accelerate Video LLMs by effectively reducing spatiotemporal redundancy. Through a comprehensive analysis of video tokens from both temporal context and visual context, FastVID dynamically partitions videos into temporally ordered segments and employs density-based token pruning within each segment. Extensive experiments across multiple Video LLMs and benchmarks demonstrate its generalization ability and effectiveness. Crucially, FastVID maintains high performance even under extreme compression rates, enabling practical deployment of fast Video LLMs.

## References

- [1] Josh Achiam, Steven Adler, Sandhini Agarwal, Lama Ahmad, Ilge Akkaya, Florencia Leoni Aleman, Diogo Almeida, Janko Altenschmidt, Sam Altman, Shyamal Anadkat, et al. Gpt-4 technical report. *arXiv preprint arXiv:2303.08774*, 2023.
- [2] Joshua Ainslie, James Lee-Thorp, Michiel De Jong, Yury Zemlyanskiy, Federico Lebrón, and Sumit Sanghai. Gqa: Training generalized multi-query transformer models from multi-head checkpoints. *arXiv preprint arXiv:2305.13245*, 2023.
- [3] Jean-Baptiste Alayrac, Jeff Donahue, Pauline Luc, Antoine Miech, Iain Barr, Yana Hasson, Karel Lenc, Arthur Mensch, Katherine Millican, Malcolm Reynolds, et al. Flamingo: a visual language model for few-shot learning. *Advances in Neural Information Processing Systems*, 2022.
- [4] Daniel Bolya, Cheng-Yang Fu, Xiaoliang Dai, Peizhao Zhang, Christoph Feichtenhofer, and Judy Hoffman. Token merging: Your vit but faster. In *Proceedings of the International Conference on Learning Representations*, 2023.
- [5] Liang Chen, Haozhe Zhao, Tianyu Liu, Shuai Bai, Junyang Lin, Chang Zhou, and Baobao Chang. An image is worth 1/2 tokens after layer 2: Plug-and-play inference acceleration for large vision-language models. In *Proceedings of the European Conference on Computer Vision*, 2024.
- [6] Zhe Chen, Weiyun Wang, Yue Cao, Yangzhou Liu, Zhangwei Gao, Erfei Cui, Jinguo Zhu, Shenglong Ye, Hao Tian, Zhaoyang Liu, et al. Expanding performance boundaries of open-source multimodal models with model, data, and test-time scaling. *arXiv preprint arXiv:2412.05271*, 2024.
- [7] Wei-Lin Chiang, Zhuohan Li, Zi Lin, Ying Sheng, Zhanghao Wu, Hao Zhang, Lianmin Zheng, Siyuan Zhuang, Yonghao Zhuang, Joseph E Gonzalez, et al. Vicuna: An open-source chatbot impressing gpt-4 with 90%\* chatgpt quality, 2023. URL <https://vicuna.1msys.org>.
- [8] Tri Dao, Dan Fu, Stefano Ermon, Atri Rudra, and Christopher Ré. Flashattention: Fast and memory-efficient exact attention with io-awareness. *Advances in Neural Information Processing Systems*, 2022.
- [9] Alexey Dosovitskiy, Lucas Beyer, Alexander Kolesnikov, Dirk Weissenborn, Xiaohua Zhai, Thomas Unterthiner, Mostafa Dehghani, Matthias Minderer, Georg Heigold, Sylvain Gelly, et al. An image is worth 16x16 words: Transformers for image recognition at scale. *arXiv preprint arXiv:2010.11929*, 2020.
- [10] Mingjing Du, Shifei Ding, and Hongjie Jia. Study on density peaks clustering based on k-nearest neighbors and principal component analysis. *Knowledge-Based Systems*, 99:135–145, 2016.
- [11] Chaoyou Fu, Yuhang Dai, Yongdong Luo, Lei Li, Shuhuai Ren, Renrui Zhang, Zihan Wang, Chenyu Zhou, Yunhang Shen, Mengdan Zhang, et al. Video-mme: The first-ever comprehensive evaluation benchmark of multi-modal llms in video analysis. In *Proceedings of the IEEE Conference on Computer Vision and Pattern Recognition*, 2025.
- [12] Tianyu Fu, Tengxuan Liu, Qinghao Han, Guohao Dai, Shengen Yan, Huazhong Yang, Xuefei Ning, and Yu Wang. Framefusion: Combining similarity and importance for video token reduction on large visual language models. *arXiv preprint arXiv:2501.01986*, 2024.
- [13] Xiaohu Huang, Hao Zhou, and Kai Han. Prunevid: Visual token pruning for efficient video large language models. *arXiv preprint arXiv:2412.16117*, 2024.
- [14] Andrew Jaegle, Felix Gimeno, Andy Brock, Oriol Vinyals, Andrew Zisserman, and Joao Carreira. Perceiver: General perception with iterative attention. In *Proceedings of the International Conference on Machine Learning*, 2021.
- [15] Peng Jin, Ryuichi Takanobu, Wancai Zhang, Xiaochun Cao, and Li Yuan. Chat-univi: Unified visual representation empowers large language models with image and video understanding. In *Proceedings of the IEEE Conference on Computer Vision and Pattern Recognition*, 2024.

[16] Bo Li, Yuanhan Zhang, Dong Guo, Renrui Zhang, Feng Li, Hao Zhang, Kaichen Zhang, Peiyuan Zhang, Yanwei Li, Ziwei Liu, et al. Llava-onevision: Easy visual task transfer. *arXiv preprint arXiv:2408.03326*, 2024.

[17] Junnan Li, Dongxu Li, Silvio Savarese, and Steven Hoi. Blip-2: Bootstrapping language-image pre-training with frozen image encoders and large language models. In *Proceedings of the International Conference on Machine Learning*, 2023.

[18] Kunchang Li, Yali Wang, Yinan He, Yizhuo Li, Yi Wang, Yi Liu, Zun Wang, Jilan Xu, Guo Chen, Ping Luo, et al. Mvbench: A comprehensive multi-modal video understanding benchmark. In *Proceedings of the IEEE/CVF Conference on Computer Vision and Pattern Recognition*, pages 22195–22206, 2024.

[19] Bin Lin, Yang Ye, Bin Zhu, Jiaxi Cui, Munan Ning, Peng Jin, and Li Yuan. Video-llava: Learning united visual representation by alignment before projection. *arXiv preprint arXiv:2311.10122*, 2023.

[20] Aixin Liu, Bei Feng, Bin Wang, Bingxuan Wang, Bo Liu, Chenggang Zhao, Chengqi Deng, Chong Ruan, Damai Dai, Daya Guo, et al. Deepseek-v2: A strong, economical, and efficient mixture-of-experts language model. *arXiv preprint arXiv:2405.04434*, 2024.

[21] Haotian Liu, Chunyuan Li, Yuheng Li, and Yong Jae Lee. Improved baselines with visual instruction tuning. In *Proceedings of the IEEE Conference on Computer Vision and Pattern Recognition*, 2024.

[22] Haotian Liu, Chunyuan Li, Yuheng Li, Bo Li, Yuanhan Zhang, Sheng Shen, and Yong Jae Lee. Llava-next: Improved reasoning, ocr, and world knowledge, January 2024. URL <https://llava-v1.github.io/blog/2024-01-30-llava-next/>.

[23] Haotian Liu, Chunyuan Li, Qingyang Wu, and Yong Jae Lee. Visual instruction tuning. *Advances in Neural Information Processing Systems*, 2024.

[24] Muhammad Maaz, Hanoona Rasheed, Salman Khan, and Fahad Shahbaz Khan. Video-chatgpt: Towards detailed video understanding via large vision and language models. In *Association for Computational Linguistics*, 2024.

[25] Alec Radford, Jong Wook Kim, Chris Hallacy, Aditya Ramesh, Gabriel Goh, Sandhini Agarwal, Girish Sastry, Amanda Askell, Pamela Mishkin, Jack Clark, et al. Learning transferable visual models from natural language supervision. In *Proceedings of the International Conference on Machine Learning*, 2021.

[26] Alex Rodriguez and Alessandro Laio. Clustering by fast search and find of density peaks. *science*, 344(6191):1492–1496, 2014.

[27] Amir Shahroudy, Jun Liu, Tian-Tsong Ng, and Gang Wang. Ntu rgb+ d: A large scale dataset for 3d human activity analysis. In *Proceedings of the IEEE Conference on Computer Vision and Pattern Recognition*, 2016.

[28] Yuzhang Shang, Mu Cai, Bingxin Xu, Yong Jae Lee, and Yan Yan. Llava-prumerge: Adaptive token reduction for efficient large multimodal models. *arXiv preprint arXiv:2403.15388*, 2024.

[29] Leqi Shen, Tianxiang Hao, Sicheng Zhao, Yifeng Zhang, Pengzhang Liu, Yongjun Bao, and Guiguang Ding. Tempme: Video temporal token merging for efficient text-video retrieval. In *Proceedings of the International Conference on Learning Representations*, 2025.

[30] Xiaoqian Shen, Yunyang Xiong, Changsheng Zhao, Lemeng Wu, Jun Chen, Chenchen Zhu, Zechun Liu, Fanyi Xiao, Balakrishnan Varadarajan, Florian Bordes, et al. Longvu: Spatiotemporal adaptive compression for long video-language understanding. In *Proceedings of the International Conference on Machine Learning*, 2025.

[31] Enxin Song, Wenhao Chai, Guanhong Wang, Yucheng Zhang, Haoyang Zhou, Feiyang Wu, Haozhe Chi, Xun Guo, Tian Ye, Yanting Zhang, et al. Moviechat: From dense token to sparse memory for long video understanding. In *Proceedings of the IEEE Conference on Computer Vision and Pattern Recognition*, 2024.

[32] Jianlin Su, Murtadha Ahmed, Yu Lu, Shengfeng Pan, Wen Bo, and Yunfeng Liu. Roformer: Enhanced transformer with rotary position embedding. *Neurocomputing*, 568:127063, 2024.

[33] Keda Tao, Can Qin, Haoxuan You, Yang Sui, and Huan Wang. Dycoke: Dynamic compression of tokens for fast video large language models. In *Proceedings of the IEEE Conference on Computer Vision and Pattern Recognition*, 2025.

[34] Rohan Taori, Ishaan Gulrajani, Tianyi Zhang, Yann Dubois, Xuechen Li, Carlos Guestrin, Percy Liang, and Tatsunori B Hashimoto. Stanford alpaca: An instruction-following llama model, 2023.

[35] Gemini Team, Rohan Anil, Sebastian Borgeaud, Jean-Baptiste Alayrac, Jiahui Yu, Radu Soricut, Johan Schalkwyk, Andrew M Dai, Anja Hauth, Katie Millican, et al. Gemini: a family of highly capable multimodal models. *arXiv preprint arXiv:2312.11805*, 2023.

[36] Ao Wang, Fengyuan Sun, Hui Chen, Zijia Lin, Jungong Han, and Guiguang Ding. [cls] token tells everything needed for training-free efficient mllms. *arXiv preprint arXiv:2412.05819*, 2024.

[37] Peng Wang, Shuai Bai, Sinan Tan, Shijie Wang, Zhihao Fan, Jinze Bai, Keqin Chen, Xuejing Liu, Jialin Wang, Wenbin Ge, et al. Qwen2-vl: Enhancing vision-language model’s perception of the world at any resolution. *arXiv preprint arXiv:2409.12191*, 2024.

[38] Haoning Wu, Dongxu Li, Bei Chen, and Junnan Li. Longvideobench: A benchmark for long-context interleaved video-language understanding. *Advances in Neural Information Processing Systems*, 37:28828–28857, 2025.

[39] Long Xing, Qidong Huang, Xiaoyi Dong, Jiajie Lu, Pan Zhang, Yuhang Zang, Yuhang Cao, Conghui He, Jiaqi Wang, Feng Wu, et al. Pyramiddrop: Accelerating your large vision-language models via pyramid visual redundancy reduction. In *Proceedings of the IEEE Conference on Computer Vision and Pattern Recognition*, 2025.

[40] Lin Xu, Yilin Zhao, Daquan Zhou, Zhijie Lin, See Kiong Ng, and Jiashi Feng. Pllava: Parameter-free llava extension from images to videos for video dense captioning. *arXiv preprint arXiv:2404.16994*, 2024.

[41] An Yang, Baosong Yang, Binyuan Hui, Bo Zheng, Bowen Yu, Chang Zhou, Chengpeng Li, Chengyuan Li, Dayiheng Liu, Fei Huang, et al. Qwen2 technical report. *arXiv preprint arXiv:2407.10671*, 2024.

[42] Senqiao Yang, Yukang Chen, Zhuotao Tian, Chengyao Wang, Jingyao Li, Bei Yu, and Jiaya Jia. Visionzip: Longer is better but not necessary in vision language models. In *Proceedings of the IEEE Conference on Computer Vision and Pattern Recognition*, 2025.

[43] Xiaohua Zhai, Basil Mustafa, Alexander Kolesnikov, and Lucas Beyer. Sigmoid loss for language image pre-training. In *Proceedings of the International Conference on Computer Vision*, 2023.

[44] Kaichen Zhang, Bo Li, Peiyuan Zhang, Fanyi Pu, Joshua Adrian Cahyono, Kairui Hu, Shuai Liu, Yuanhan Zhang, Jingkang Yang, Chunyuan Li, et al. Lmms-eval: Reality check on the evaluation of large multimodal models. In *Findings of the Association for Computational Linguistics: NAACL*, 2025.

[45] Qizhe Zhang, Aosong Cheng, Ming Lu, Zhiyong Zhuo, Minqi Wang, Jiajun Cao, Shaobo Guo, Qi She, and Shanghang Zhang. [cls] attention is all you need for training-free visual token pruning: Make vlm inference faster. *arXiv preprint arXiv:2412.01818*, 2024.

[46] Yuan Zhang, Chun-Kai Fan, Junpeng Ma, Wenzhao Zheng, Tao Huang, Kuan Cheng, Denis Gudovskiy, Tomoyuki Okuno, Yohei Nakata, Kurt Keutzer, et al. Sparsevlm: Visual token sparsification for efficient vision-language model inference. In *Proceedings of the International Conference on Machine Learning*, 2025.

[47] Yuanhan Zhang, Jinming Wu, Wei Li, Bo Li, Zejun Ma, Ziwei Liu, and Chunyuan Li. Video instruction tuning with synthetic data. *arXiv preprint arXiv:2410.02713*, 2024.

- [48] Junjie Zhou, Yan Shu, Bo Zhao, Boya Wu, Shitao Xiao, Xi Yang, Yongping Xiong, Bo Zhang, Tiejun Huang, and Zheng Liu. Mlvu: A comprehensive benchmark for multi-task long video understanding. In *Proceedings of the IEEE Conference on Computer Vision and Pattern Recognition*, 2025.
- [49] Orr Zohar, Xiaohan Wang, Yann Dubois, Nikhil Mehta, Tong Xiao, Philippe Hansen-Estruch, Licheng Yu, Xiaofang Wang, Felix Juefei-Xu, Ning Zhang, et al. Apollo: An exploration of video understanding in large multimodal models. *arXiv preprint arXiv:2412.10360*, 2024.

## Appendix

This appendix provides additional details and results to support our main paper:

- Section A presents additional experimental settings, including reproduction details of the compared baselines and an estimation of the computational cost.
- Section B presents additional experimental results, such as ablation studies on key hyperparameters, further qualitative results, and results on **Qwen2-VL** [37].
- Section C discusses limitations of our approach and its potential broader impacts.

## A Additional Experimental Settings

### A.1 Reproduction Details of Compared Baselines

All experiments are conducted using LMMs-Eval<sup>2</sup> [44] for consistency. The performance of the vanilla versions of LLaVA-OneVision<sup>3</sup> [16], LLaVA-Video<sup>3</sup> [47], and Qwen2-VL<sup>4</sup> [37] differs slightly from their reported results, remaining within an acceptable margin of error. We reimplement all baseline methods using LMMs-Eval, following their official implementations:

- **FastV<sup>5</sup>** [5] (**ECCV 2024**). FastV performs token pruning at the  $K$ -th layer of the LLM using attention scores, with a filtering ratio  $R$ . We reimplement it with  $K = 2$ , using  $R \in \{75\%, 80\%, 85\%, 90\%\}$  in Table 1 and  $R \in \{75\%, 90\%\}$  in Table 2.
- **VisionZip<sup>6</sup>** [42] (**CVPR 2025**). Visionzip performs pruning at the vision encoder’s output, which conflicts with pooling operations in Video LLMs and degrades performance. To address this, we implement VisionZip\*, which applies pruning after pooling. Following the original settings, each frame retains both dominant and contextual tokens in a 54:10 ratio. We define  $r$  as the proportion of tokens retained per frame. We set  $r \in \{25\%, 20\%, 15\%, 10\%\}$  in Table 1 and  $r \in \{25\%, 10\%\}$  in Table 2.
- **DyCoke<sup>7</sup>** [33] (**CVPR 2025**). DyCoke prunes in both prefilling and decoding stages. For fair comparison, we only evaluate its pre-filling stage. The pruning rate in the TTM module is set  $K \in \{0.9, 1.0\}$  in both Table 1 and Table 2.
- **PruneVID<sup>8</sup>** [13] (**ACL 2025**). PruneVID includes both input-stage and intra-LLM pruning in the pre-filling phase, along with decoding pruning. For fair comparison, we evaluate two variants: PruneVID\* (input-stage pruning only) and PruneVID (full prefilling pruning). Following the original settings, we use a threshold  $\tau = 0.8$ , temporal segment ratio  $\gamma = 0.25$ , token selection ratio  $\alpha = 0.4$ , and attention calculations use the 10th layer. The cluster ratio  $\beta$  controls compression in the input-stage pruning. We use  $\beta = 11\%$  in Table 1 and Table 3.

### A.2 Computational Cost Estimation

Following prior works [5, 39], we report the theoretical FLOPs of the LLM related to visual/video tokens. Specifically, LLaVA-OneVision [16], LLaVA-Video [47], and Qwen2-VL [37] are all built on Qwen2 [41], which employs grouped-query attention [2] and a three-layer FFN structure. The per-layer FLOPs of the LLM are computed as:

$$2nD(h_{kv}d) + 2nD^2 + 2n^2D + 3nDD' \quad (6)$$

where  $n$  is the number of video tokens,  $D$  is the hidden state size,  $D'$  is the FFN intermediate size,  $h_{kv}$  is the number of key/value heads, and  $d$  is the head dimension.

<sup>2</sup><https://github.com/EvolvingLMMs-Lab/lmms-eval>, MIT License

<sup>3</sup><https://github.com/LLaVA-VL/LLaVA-NeXT>, Apache License 2.0

<sup>4</sup><https://github.com/QwenLM/Qwen2.5-VL>, Apache License 2.0

<sup>5</sup><https://github.com/pkunlp-icler/FastV>

<sup>6</sup><https://github.com/dvlab-research/VisionZip>, Apache License 2.0

<sup>7</sup><https://github.com/KD-TAO/DyCoke>, Apache License 2.0

<sup>8</sup><https://github.com/Visual-AI/PruneVid>, CC BY-NC-SA 4.0 License

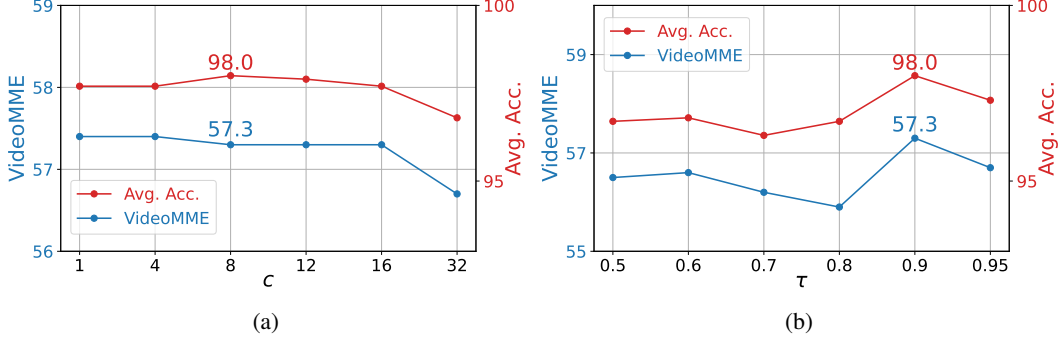


Figure 6: Ablation study on  $c$  and  $\tau$  in DySeg.  $c$  denotes the minimum number of segments in a video, whereas  $\tau$  denotes the transition similarity threshold. Both parameters jointly control the segmentation granularity.

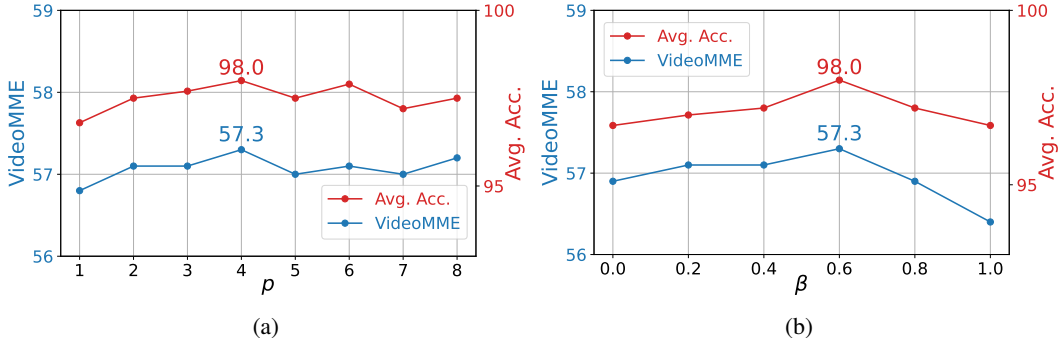


Figure 7: Ablation study on  $p$  and  $\beta$  in DTM.  $p$  denotes the interval for anchor frame selection, whereas  $\beta$  controls the merging weight for anchor tokens and their associated tokens in Eq. (5).

## B Additional Experimental Results

### B.1 Ablation study on $c$ and $\tau$ in DySeg

We evaluate the effect of  $c$  and  $\tau$  in Eq. (2) of DySeg. Figure 6(a) shows results with varying  $c$ . In simple video scenarios with high transition similarity,  $c$  regulates segmentation. When  $c = 1$ , segmentation relies solely on  $\tau$ .  $c = 32$  divides the video into single-frame segments. Performance remains stable for  $1 \leq c \leq 16$ , but the decline at  $c = 32$  suggests that excessive segmentation disregards temporal relationships. The optimal performance at  $c = 8$  indicates the benefit of a minimum cluster number. Figure 6(b) shows results with varying  $\tau$ . When  $\tau$  is small, most transitions in  $S$  are selected by  $c$ . As  $\tau$  increases, more transitions fall below the threshold. The best performance is achieved at  $\tau = 0.9$ , effectively grouping redundant frames while separating non-redundant ones.

### B.2 Ablation study on $p$ and $\beta$ in DTM

In Figure 7(a), we evaluate the effect of  $p$  on anchor frame selection, from which anchor tokens are subsequently sampled. When  $p = 1$ , anchor tokens are evenly distributed across all frames within a segment. As  $p$  increases, fewer frames are selected as anchors, while more anchor tokens are allocated to each anchor frame. Given the high similarity between frames in a segment, a sufficient number of anchor tokens per anchor frame is essential to capture visual context. However, if  $p$  is too large, all anchor tokens come from the first frame, limiting temporal information. We find that  $p = 4$  yields the best performance by effectively capturing spatiotemporal context. Figure 7(b) shows the effect of  $\beta$  in Eq. (5). When  $\beta = 0.0$ , matching tokens are averaged.  $\beta = 1.0$  discards all non-anchor tokens, removing segment visual context and leading to a performance drop. Notably, Anchor-centric Assignment (when  $\beta = 0.6$ ) yields optimal results, highlighting the importance of representative tokens and visual context.

Table 7: Comparison of state-of-the-art methods on Qwen2-VL [37]. A/B in # Tokens indicates that A tokens are provided as input to the LLM, and subsequently compressed to B tokens during the LLM forward pass. FastV performs pruning based on LLM attention scores, but its eager-attention implementation materializes the full attention matrix in memory, leading to OOM errors due to the large number of video tokens.

Method	# Token	TFLOPs	VideoMME						
			Short	Medium	Long	Overall			
Vanilla	13447.1	100%	124.04	100%	74.1	60.4	54.3	63.0	100%
FastV [5]ECCV'24	13447.1/3361.8	100%/25%	31.34	25.3%	Out of Memory				
VisionZip* [42]CVPR'25	3349.3	24.9%	24.11	19.4%	70.9	56.3	48.3	58.5	92.9%
PruneVID* [13]ACL'25	3460.6	25.7%	24.99	20.1%	66.7	54.0	48.1	56.3	89.4%
<b>FastVID</b>	3349.3	24.9%	24.11	19.4%	<b>72.7</b>	<b>58.3</b>	<b>50.7</b>	<b>60.6</b>	<b>96.2%</b>

### B.3 Additional Qualitative Results

Figures 8-10 show additional qualitative results on VideoMME. We use the following settings:  $c = 0$ ,  $\tau = 0.9$ ,  $d = 0.4$ ,  $p = 2$ , retaining an average of 10 tokens per frame. Figure 8 presents static scenes, while Figures 9 and 10 present dynamic scenes. These visualizations demonstrate FastVID’s ability to adaptively segment videos across varying temporal dynamics. Within each segment, the merged region boundaries loosely align with object shapes, highlighting the effectiveness of the proposed DTM in preserving visual context.

### B.4 Results on Qwen2-VL

Unlike LLaVA-OneVision [16] and LLaVA-Video [47], Qwen2-VL [37] employs a distinct architecture that samples 768 frames per video and processes them using 3D convolutions. It introduces M-RoPE, which decomposes rotary embeddings into temporal, height, and width components. The model dynamically adjusts the resolution of each frame. In Table 7, our FastVID outperforms other baselines on Qwen2-VL under similar model complexity. In particular, FastVID achieves a **2.4** accuracy improvement on the long subset. As shown in Tables 1, 2, and 7, our FastVID’s consistent superiority across three distinct Video LLM architectures further validates its strong generalizability and practical effectiveness.

## C Additional Discussions

### C.1 Limitations

FastVID achieves strong performance on LLaVA-OneVision [16] (**32** frames/video), maintaining comparable accuracy with only **8.3%** of the FLOPs. However, on LLaVA-Video [47] (**64** frames/video) and Qwen2-VL [37] (**768** frames/video), although FastVID consistently outperforms existing SoTA baselines, a noticeable accuracy drop occurs compared to the original model. We hypothesize that this is primarily due to the increased number of sampled frames, which leads to fewer tokens per frame and increases the semantic importance of each token. Consequently, aggressive pruning risks discarding critical information. In addition, although our query-agnostic token pruning effectively reduces spatiotemporal redundancy, it fails to emphasize query-relevant information sparsely distributed across extensively sampled frames. To overcome these challenges, future work may explore integrating text-guided keyframe selection to better support long-frame Video LLMs [37, 47].

### C.2 Broader Impacts

FastVID accelerates inference for existing Video LLMs without modifying their parameters or training new models, thereby minimizing the risk of introducing new biases or unintended behaviors. However, FastVID inherits any potential negative societal impacts of the original models, such as representational bias or potential misuse. Despite this, FastVID maintains strong performance even under extreme token compression. This makes the use of Video LLMs more practical in environments with limited computational resources, promoting broader and more sustainable deployment.

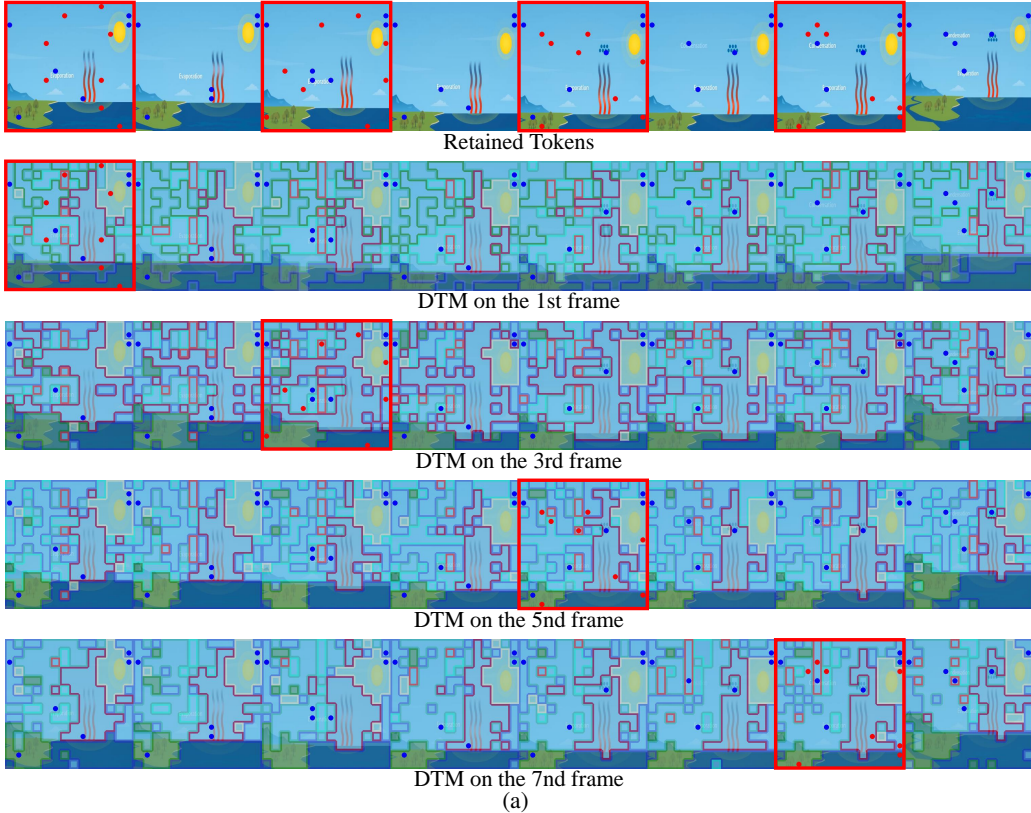


Figure 8: Segment boundaries are marked by brown vertical lines. Tokens generated by DTM and ATS are highlighted in red and blue, respectively. Anchor frames, indicated by red boxes, are processed by DTM individually. In DTM, patches with matching inner and border colors are merged.

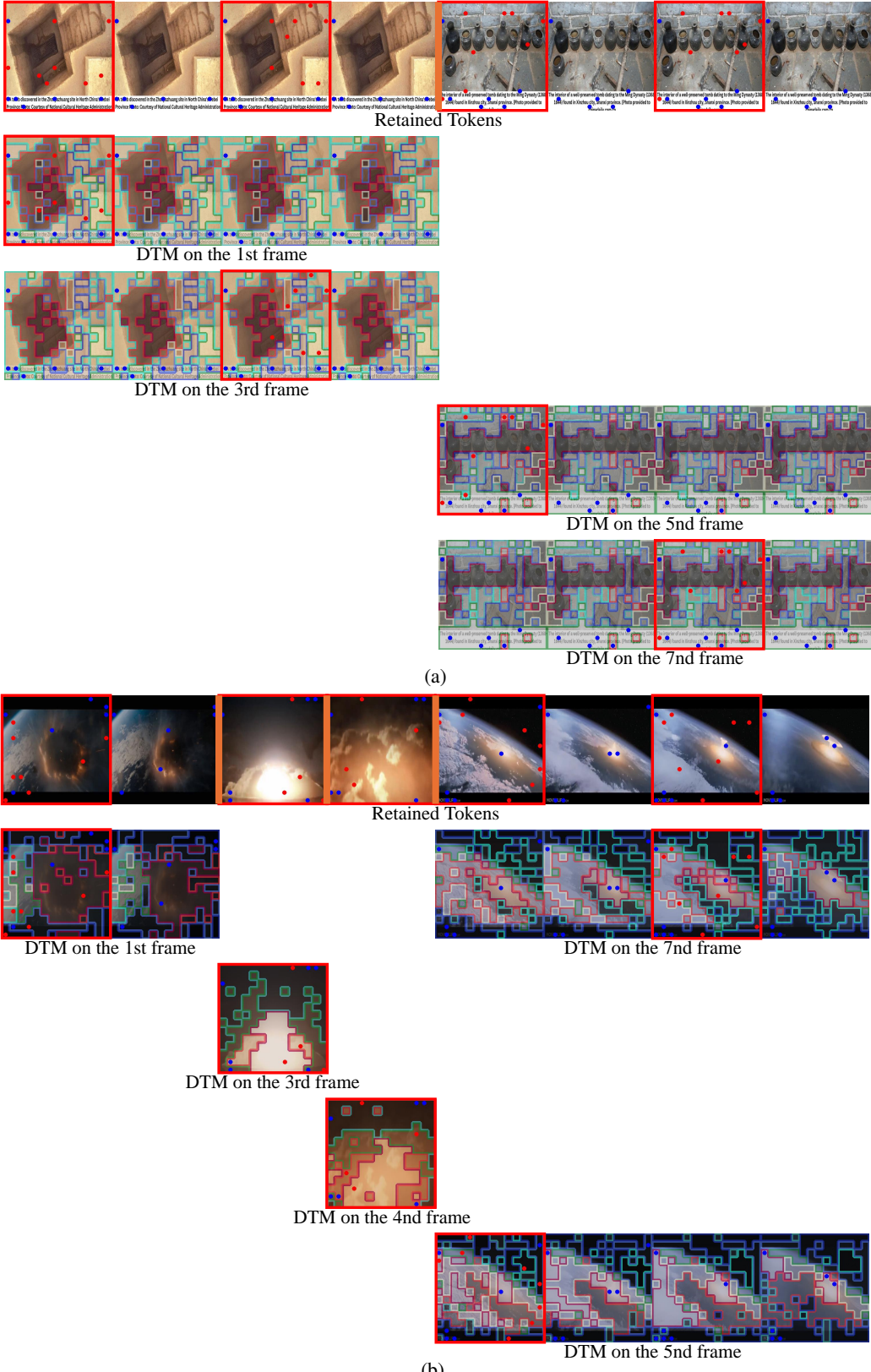


Figure 9: Segment boundaries are marked by brown vertical lines. Tokens generated by DTM and ATS are highlighted in red and blue, respectively. Anchor frames, indicated by red boxes, are processed by DTM individually. In DTM, patches with matching inner and border colors are merged.

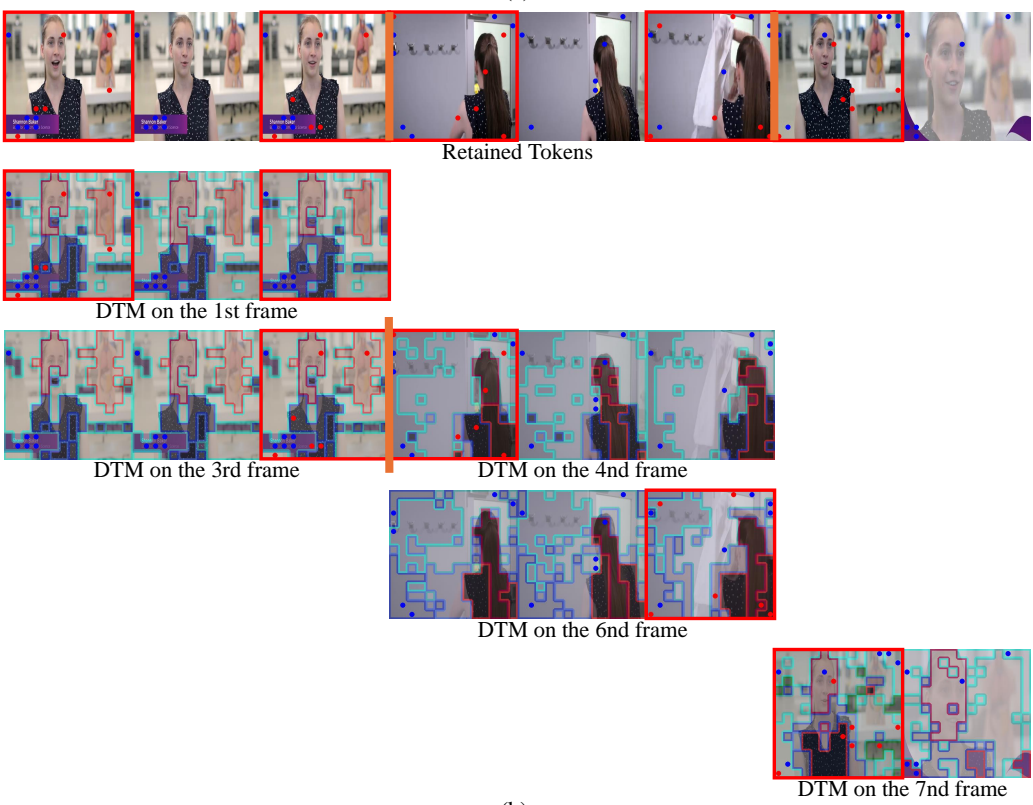
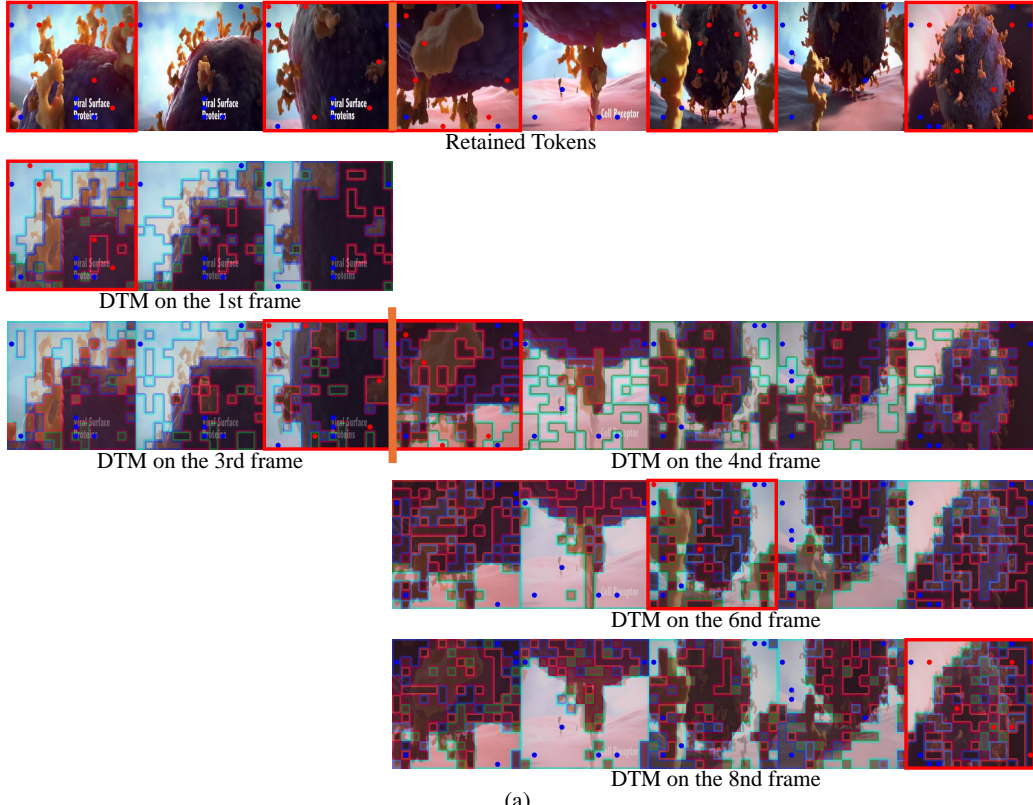


Figure 10: Segment boundaries are marked by brown vertical lines. Tokens generated by DTM and ATS are highlighted in red and blue, respectively. Anchor frames, indicated by red boxes, are processed by DTM individually. In DTM, patches with matching inner and border colors are merged.